

RL-TR-97-159
Final Technical Report
October 1997



OPTICAL CLOCK RECOVERY USING MODELOCKED SEMICONDUCTOR DIODE LASERS

University of Central Florida

Peter J. Delfyett and Brian Mathason

APPROVED FOR PUBLIC RELEASE; DISTRIBUTION UNLIMITED.

19980217 498

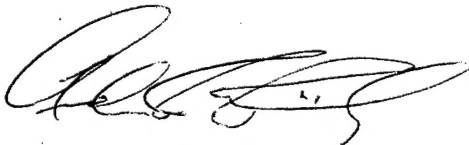
DTIC SECURITY INSPECTED 4

**Rome Laboratory
Air Force Materiel Command
Rome, New York**

This report has been reviewed by the Rome Laboratory Public Affairs Office (PA) and is releasable to the National Technical Information Service (NTIS). At NTIS it will be releasable to the general public, including foreign nations.

RL-TR-97-159 has been reviewed and is approved for publication.

APPROVED:



ANDREW R. PIRICH
Project Engineer

FOR THE DIRECTOR:



DONALD W. HANSON, Director
Surveillance & Photonics Directorate

If your address has changed or if you wish to be removed from the Rome Laboratory mailing list, or if the addressee is no longer employed by your organization, please notify RL/OCPA, 25 Electronic Pky, Rome, NY 13441-4515. This will assist us in maintaining a current mailing list.

Do not return copies of this report unless contractual obligations or notices on a specific document require that it be returned.

REPORT DOCUMENTATION PAGE			Form Approved OMB No. 0704-0188	
Public reporting burden for this collection of information is estimated to average 1 hour per response, including the time for reviewing instructions, searching existing data sources, gathering and maintaining the data needed, and completing and reviewing the collection of information. Send comments regarding this burden estimate or any other aspect of this collection of information, including suggestions for reducing this burden, to Washington Headquarters Services, Directorate for Information Operations and Reports, 1215 Jefferson Davis Highway, Suite 1204, Arlington, VA 22202-4302, and to the Office of Management and Budget, Paperwork Reduction Project (0704-0188), Washington, DC 20503.				
1. AGENCY USE ONLY (Leave blank)		2. REPORT DATE Oct 97		3. REPORT TYPE AND DATES COVERED FINAL Sep 96 - Mar 97
4. TITLE AND SUBTITLE OPTICAL CLOCK RECOVERY USING MODELOCKED SEMICONDUCTOR DIODE LASERS			5. FUNDING NUMBERS C - F30602-96-2-0200 PE - 62702F PR - 4600 TA - P5 WU - PR	
6. AUTHOR(S) Peter J. Delfyett, Brian Mathason				
7. PERFORMING ORGANIZATION NAME(S) AND ADDRESS(ES) University of Central Florida Center for Research and Education in Optics and Lasers (CREOL) Division of Sponsored Research 4000 Central Florida Boulevard, ADM 243 Orlando FL 32816-0150			8. PERFORMING ORGANIZATION REPORT NUMBER	
9. SPONSORING / MONITORING AGENCY NAME(S) AND ADDRESS(ES) Rome Laboratory/OCPA 25 Electronic Pky Rome NY 13441-4515			10. SPONSORING / MONITORING AGENCY REPORT NUMBER RL-TR-97-159	
11. SUPPLEMENTARY NOTES Rome Laboratory Project Engineer: Andrew R. Pirich, OCPA (315) 330-4147				
12a. DISTRIBUTION AVAILABILITY STATEMENT Approved for Public Release; Distribution Unlimited			12b. DISTRIBUTION CODE	
13. ABSTRACT (Maximum 200 words) Ultrahigh speed photonic networks require accurate methods of synchronization in order to provide control signals for switching, routing and demultiplexing. This final report describes work which utilizes external cavity passively modelocked semiconductor lasers as all optical clock recovery oscillators. It is demonstrated that these lasers can be used to extract and generate accurate timing signals synchronized to an incoming data signal. The results show that minimum injection powers of a few microwatts can be employed for accurate clock recovery.				
14. SUBJECT TERMS timing jitter, traveling wave amplifiers (TWA), time domain multiplexing (TDM), wavelength division multiplexing (WDM), multiple quantum well (MQW) saturable absorber, longitudinal modes			15. NUMBER OF PAGES 28	
			16. PRICE CODE	
17. SECURITY CLASSIFICATION OF REPORT UNCLASSIFIED	18. SECURITY CLASSIFICATION OF THIS PAGE UNCLASSIFIED	19. SECURITY CLASSIFICATION OF ABSTRACT UNCLASSIFIED	20. LIMITATION OF ABSTRACT UNLIMITED	

Table of Contents

1.0 Introduction	page 1
2.0 The Optical Clock Recovery Experimental System	page 1
3.0 Theory of Operation	page 5
4.0 Timing Jitter	page 6
4.1 Measuring Timing Jitter	page 6
4.2 Timing Jitter vs. Injected Power	page 10
4.3 Timing Jitter vs. Frequency Detuning	page 11
4.4 Timing Jitter vs. Wavelength Detuning	page 12
4.5 Timing Jitter vs. Bit Pattern	page 13
5.0 Future Work	page 15
6.0 References	page 16

Table of Figures

Figure 1: Clock Recovery Schematic Diagram	page 2
Figure 2: Modulation Characteristics of the TWA amplifier	
(a) Amplifier output with and without input power showing contrast between laser amplification and ASE	page 3
(b) Optical amplification vs. DC bias current for a fixed optical input	page 3
(c) Electrical bias pulse used to modulate the amplifier output	page 3
Figure 3: Optical pulse train from clock recovery system	page 4
Figure 4: Nonlinearity of output power due to intracavity MQW saturable absorber	page 5
Figure 5: RF Power spectrum of laser system that is	page 6
(a) passively modelocked and	
(b) hybrid modelocked	
Figure 6: Frequency squared increase in phase noise power due to timing jitter	page 7
Figure 7: RF Power spectrum for the injection modelocked clock recovery oscillator	page 8
Figure 8: Correlation scheme for measuring relative timing jitter between the transmitter and clock.	page 9

Figure 9: RF spectrum of the clock oscillator near clocking threshold shows erratic behavior page 11

Figure 10: (a) Frequency Detuning vs. Injected Power with exponential fit page 12

(b) RF spectrum at the maximum and minimum of the detuning range page 12

Figure 11: Wavelength tunable transmitter laser system page 13

Figure 12: Pulse Slicer

(a) pulses before being modulated page 14

(b) 1 out of 10 pulse slicing page 14

(c) RF Spectrum after slicing showing modulation page 14

1.0 Introduction

As the demand for higher speeds in data networks increases, the capabilities of conventional electronic circuits will be exceeded [1]. Future high speed networks may incorporate photonic techniques to provide a variety of functions, e.g., switching, processing and computing, and transmission, owing to the vast amounts of bandwidth these technologies provide [2]. Therefore, the generation of synchronized optical clocking, or timing signals is important in the development of these high speed optical networks. For time domain multiplexing systems (TDM) an optical clock recovery system is an important component. In addition, for wavelength division multiplexing systems (WDM), a clock recovery system that works robustly for multiple wavelengths would also be of value. Clearly, an efficient and robust scheme for recovering an optical clock signal from an incoming optical data stream is desirable.

Clocking signals can be extracted or regenerated from a data signal through optical, electrical or hybrid techniques. All-optical clock recovery offers the most promise for ultrafast systems because it avoids the speed limitations of electronic components. Several techniques for all-optical clock recovery have been demonstrated using external cavity semiconductor lasers [2, 3], self-pulsating laser diodes [4, 5, 6], and fiber lasers using fiber nonlinearities [7] and semiconductor nonlinearities [8].

Several optical clock recovery techniques have been demonstrated but not characterized for performance capabilities. A theoretical model of synchronization to an external pulse stream for a semiconductor laser has been reported [9], but little has been done experimentally. In this dissertation, we will experimentally characterize the dynamics of all-optical clock recovery using semiconductor traveling wave amplifiers. We will look at the timing jitter of the generated clock signal with respect to the incoming data stream and how it varies with injected power from the data signal, frequency detuning of the repetition rate, and wavelength detuning. In addition, we will measure the amount of time required for the system to generate a synchronized clocking signal subsequent to the injection of the data pulses, which we will call lock-up time. We will also measure the amount of time it takes for the system to lose synchronization after the data stops, which we will call the ring-down time.

2.0 The Optical Clock Recovery Experimental System

We have successfully constructed in our laboratory an all-optical clock recovery system using traveling wave amplifiers (TWA) in an external cavity configuration [10]. Figure 1 shows a schematic diagram of the clock recovery experiment. There are three main components to the experimental setup, the transmitter, the amplifier/modulator, and the clock recovery oscillator.

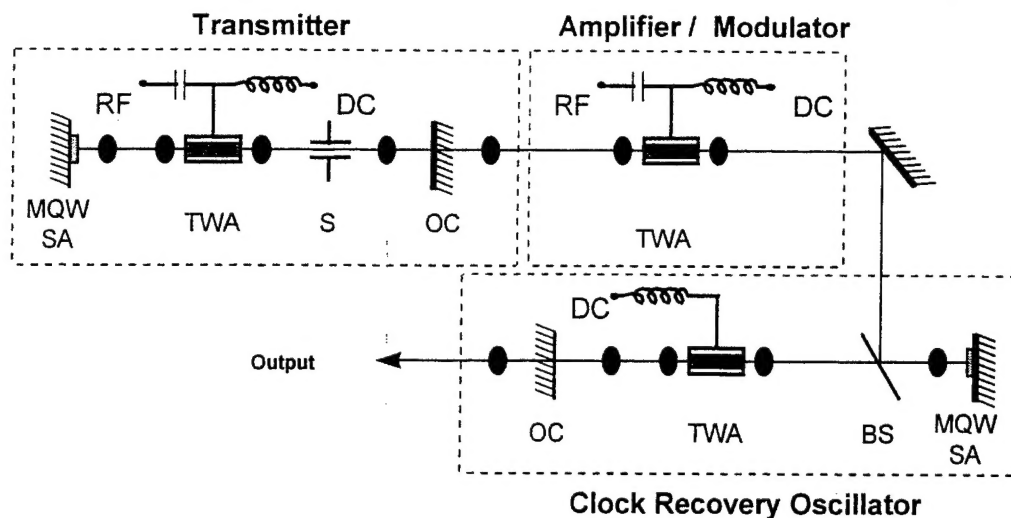


Figure 1: Clock Recovery Schematic Diagram.

The purpose of the transmitter and the amplifier is to generate the optical data stream that will be used to regenerate the clocking signal. The transmitter generates a steady stream of pulses and the amplifier increases the power and modulates the pulses into an optical data bit pattern. Though we use an almost identical system for the transmitter as the clock recovery oscillator, in a real system any transmission source can be used as long as the data pulses stay within the system limits for wavelength, repetition rate, and pulse width. The transmission source could be, for example, another node in an optical communications network, or a master clock source in a multichip module (MCM) computer.

The transmitter laser is comprised of a 350 μm long AlGaAs angled stripe traveling wave amplifier (TWA) operating at 830 nm. The TWA is placed inside a resonant cavity in which the round trip time for an optical pulse is 3.2 ns. This corresponds to a repetition rate of 311 MHz. In many commercial applications, the all-optical clock recovery oscillator would operate at higher repetition rates. However, in order to facilitate probing of the fundamental dynamics of the system, an external cavity configuration must be used with a large enough cavity to allow for additional components to be placed inside. The large cavity length constrains the achievable repetition rates. For characterizing the dynamics of the system, however, this data rate is sufficient. In our experiment, our repetition rate corresponds to the STS-6 data rate in the SONET standard.

The transmitter TWA is DC biased at 150 mA to produce CW laser output at 2-3 mW average optical power. Then we apply an RF modulation through a bias tee to actively modelock the laser. The RF modulation is frequency tuned to the cavity resonance (~ 311 MHz) to provide the optimal modelocked pulse stream. A multiple quantum well (MQW) saturable absorber [11] is placed at the rear cavity mirror to hybrid modelock the laser. The RF modulation provides temporal stability and the MQW saturable absorber provides better pulse shortening for the modelocked laser [12].

The transmitter output is coupled into a 500 μm long angle stripe TWA. This TWA is DC biased at 300 mA to amplify the output data stream to produce 20-30 mW average output power. The amplifier also generates the pulse pattern by modulating the bias current. Figure 2 shows the modulation characteristics of the amplifier. For an input power of 1.4 mW and a DC bias of 300 mA, the output power is 25.5 mW. Without the input power, the amplified spontaneous emission is 7.9 mW. This results in a contrast ratio (gain/ASE) of 2.2.

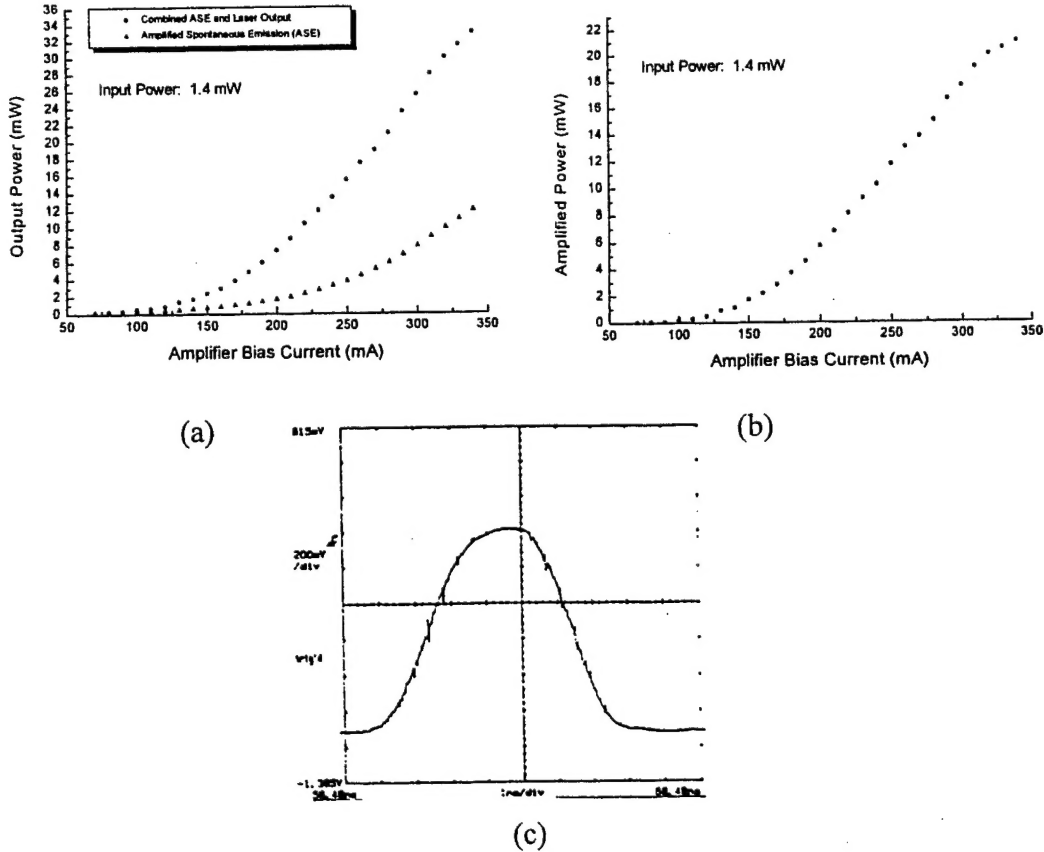


Figure 2: Modulation characteristics of the TWA amplifier. (a) Amplifier output with and without input power showing contrast between laser amplification and ASE. (b) Optical amplification vs. DC bias current for a fixed optical input. (c) Electrical bias pulse used to modulate the amplifier output.

After the amplifier, the data is ready for transfer through a data channel to the clock recovery oscillator. Typically this would be through an optical fiber, waveguide, or a network of optical interconnections. For this experiment the data stream was directly free-space coupled into the clock recovery oscillator using a pellicle beamsplitter inside the clock cavity. The beamsplitter has a nominal reflectance of 4%. An optical isolator, with greater than 30 dB extinction, frustrates unwanted feedback through the amplifier.

The clock recovery oscillator is nearly identical to the transmitter oscillator. The cavity length should be matched to the transmitter since it effects the allowable repetition rates for the system. The laser should also be passively modelocked with an identical MQW saturable absorber to assure that the data pulses will be within the excitonic absorption peak of the clocking saturable absorber. However, the clock oscillator is not synchronized with the transmitter since it has been *independently* modelocked by the saturable absorber. There will also be significant pulse to pulse timing jitter, which is characteristic of passively modelocked lasers [2]. An RF current bias is not used to reduce the timing jitter because active modelocking would stabilize the clock phase inhibiting eventual synchronization with the data stream through injection modelocking.

When the data stream is injected into the clock recovery oscillator, it will cause the pulse stream to become synchronized with the data. Figure 3 shows the optical pulse train from the all-optical clock recovery system. The clock pulses and the transmitter pulses are combined with a beamsplitter and detected by a fast photodetector. The constant phase delay between the clock and transmitter pulses shows that the signals are indeed synchronized.

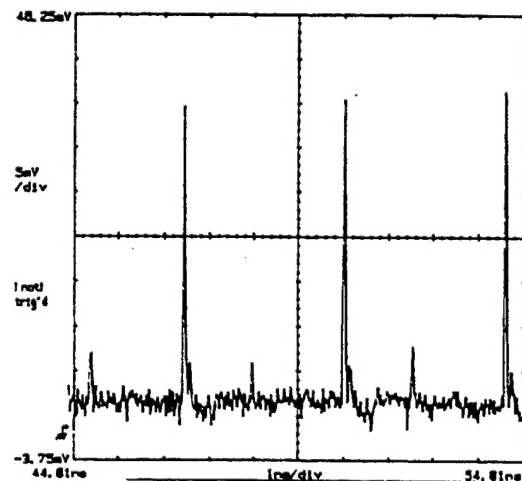


Figure 3: Optical pulse train from clock recovery system (larger pulses from clock, smaller ones from transmitter).

3.0 Theory of Operation

When a laser oscillator is operating in the CW mode, many longitudinal modes exist in the cavity [13]. These longitudinal modes have random phase with respect to each other. In modelocking, the phases of the longitudinal modes are locked together through some external mechanism. Locking the modes together causes the laser to emit a periodic train of pulses.

The MQW saturable absorber acts as a nonlinear switch inside the cavity to lock the phases of the longitudinal modes. Excitonic absorption in the absorber is strong at low intensities, but at higher intensities it becomes bleached. Since the phases of the longitudinal modes are random and fluctuating, at some instances some or all of the modes will be in phase. When this happens, it will generate a high intensity pulse that will bleach the saturable absorber and be sustained in the cavity. Thus, a pulse train will form out of the random noise fluctuations in the CW laser, and passive modelocking has occurred.

Figure 4 show that there is hysteresis in the output power of the laser system when an MQW saturable absorber is introduced into the cavity. The nonlinear effects of the saturable absorber allow us to injection modelock the laser to another oscillator. The data signal energy is injected into the cavity so that it encounters the saturable absorber. Thus the data signal modulates the saturable absorber by bleaching and the longitudinal modes existing inside the cavity are locked to the data stream.

It is also possible to exploit the nonlinear properties of the TWA. Injecting the data signal into the TWA will cause depletion of the gain as the data signal is amplified. This will frustrate passive modelocking *unless* it is synchronized with the data stream. The extra gain will also decrease the threshold injected power needed bleach the saturable absorber.

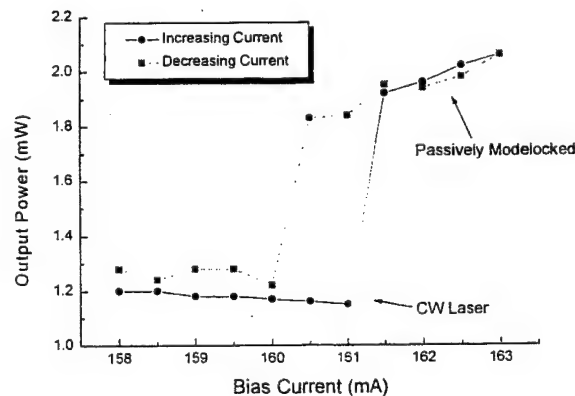


Figure 4: Nonlinearity of output power due to intracavity MQW saturable absorber.

Assuming that the external signal has the same repetition rate as the clock signal, and they are both operating at approximately the same wavelength, modulation of the saturable absorber will synchronize the clock with the data signal. One way to verify this is to observe that the phase noise sidebands on the clock signal will be eliminated. This means that the timing jitter has been reduced, which will be discussed in greater detail in the following section.

4.0 Timing Jitter

4.1 Measuring Timing Jitter

One of the most significant parameters for measuring the stability of a clocking system is the timing jitter. There are several different types of timing jitter that can be measured for a synchronized clocking system.

The pulse to pulse timing jitter of the clock oscillator is the variation in the repetition rate of the clock oscillator with respect to itself. When we measure this, we are measuring how precise the clock period is over time. This is the timing jitter that would be most significant when it is not important to mimic the jitter on the input data. A regenerator/repeater is an example of a system where this type of jitter would be important.

We use standard power spectrum techniques [¹⁴, ¹⁵] to measure the pulse to pulse timing jitter of the clock oscillator. The optical pulse train is detected with a high speed photodetector and analyzed with an RF spectrum analyzer. The temporal jitter of the pulse train manifests itself as an increase in the power contained in the phase noise sidebands of the power spectrum. Figure 5 shows the RF spectra for pulse trains from a hybrid modelocked laser system and from a passively modelocked laser system. The additional phase noise sidebands clearly shows the extra timing jitter on the passively modelocked system.

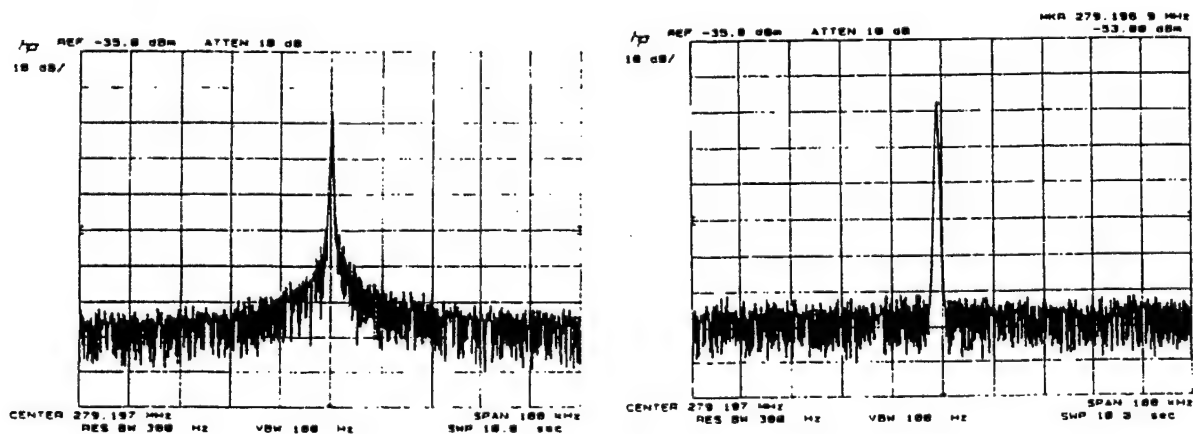


Figure 5: RF Power spectrum of laser system that is (a) passively modelocked and (b) hybrid modelocked.

The relative timing jitter can be estimated from the power spectrum by using [16]

$$\frac{\Delta T}{T} = \frac{1}{2\pi n} \left[\frac{P_S \Delta \nu}{P_C B_r} \right]^{\frac{1}{2}} \quad (1)$$

where T is the pulse period, ΔT is the variation in the pulse period, n is the harmonic number of the power spectrum being used in the measurement, P_S and P_C are the powers contained in the phase noise sideband and the carrier, respectively, $\Delta \nu$ is the -3 dB bandwidth of the phase noise sideband, and B_r is the resolution bandwidth of the spectrum analyzer. Figure 6 shows the frequency squared dependence of the phase noise sidebands, which is characteristic of timing jitter.

The timing jitter for the passively modelocked laser in Figure 5a can be estimated, using equation (1), to be 32 ps. The timing jitter for the hybrid modelocked laser in Figure 5b is more difficult to measure from this data set because the noise was smaller than the background noise of the spectrum analyzer. But assuming $\Delta \nu$ will be the same or less for the hybrid modelocked transmitter, we can estimate that the timing jitter is less than 5.7 ps. Additional measurements with better resolution bandwidth and at higher frequency harmonics have shown hybrid modelocking has, indeed, much less timing jitter, about 0.5 ps. Figure 7 shows the RF spectrum for the clock recovery oscillator after it is injection modelocked by the transmitted data stream.

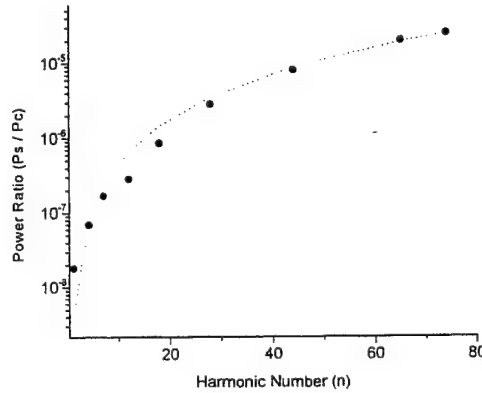


Figure 6: Frequency squared increase in phase noise power due to timing jitter.

From the phase noise sidebands in the RF spectrum shown in Figure 7, we calculate the timing jitter on the injection modelocked laser output (clock signal) to be 0.5 ps, which is comparable to the transmitter's timing jitter. Thus, the timing jitter is greatly reduced.

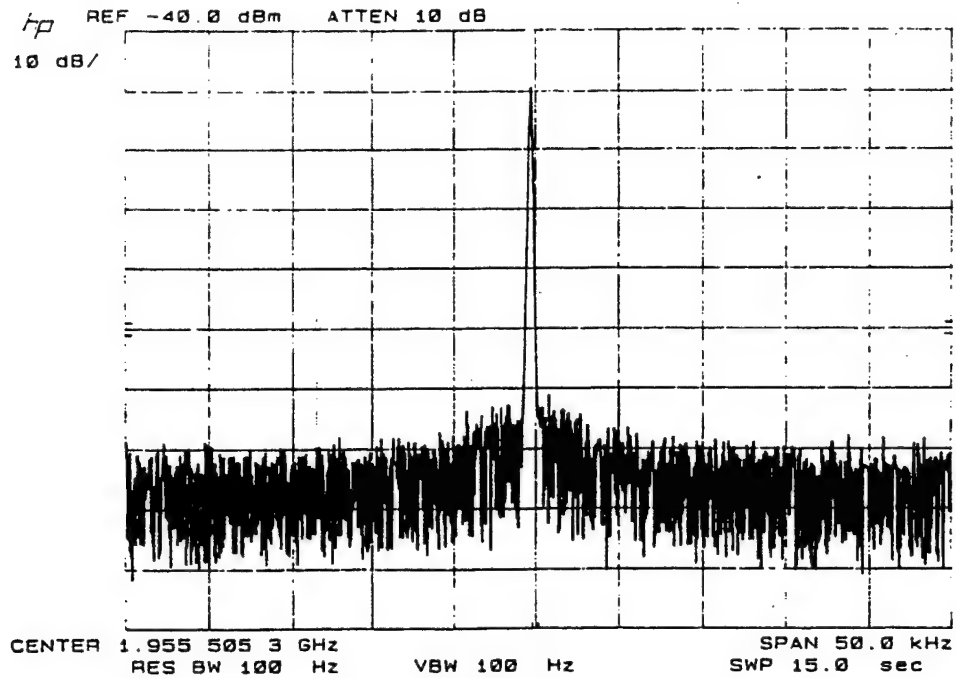


Figure 7: RF power spectrum for the injection modelocked clock recovery oscillator.

Another type of timing jitter that is important to measure is the relative timing jitter of the clock pulses *with respect to* the data pulses. This is especially important when the clock is to be used in switching or logical computation systems where the clocking pulses and data pulses must arrive at another device simultaneously. In this case, it is desirable that the clock pulses *maintain* the jitter of the data stream.

Nonlinear optical cross-correlation techniques can be used to measure the timing jitter between the clock and data stream [17]. Figure 8 shows a scheme for using correlation techniques to measure the relative pulse to pulse timing jitter between the transmitter and the clock oscillator. The transmitter and the clock oscillator output beams are both directed into an autocorrelator, with a small relative time delay, τ_d between the pulses.

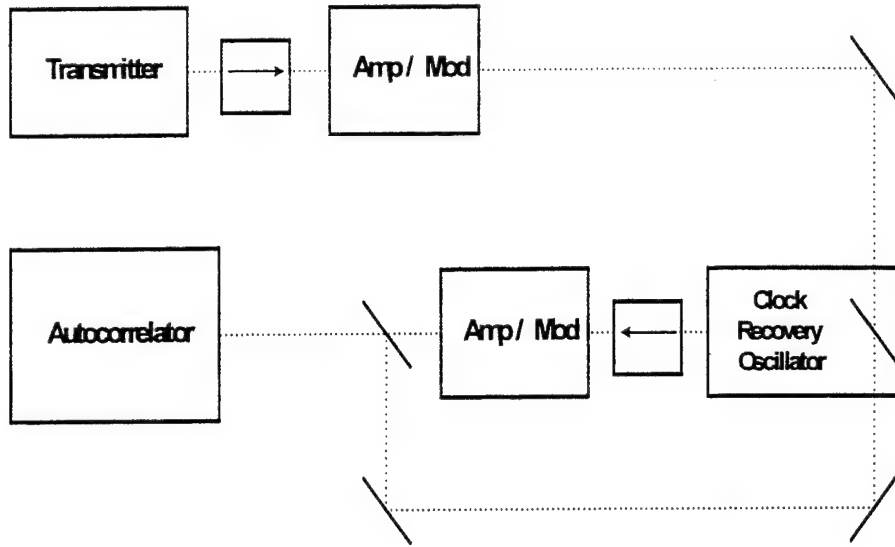


Figure 8: Correlation scheme for measuring relative timing jitter between the transmitter and clock.

Since the correlation of two pulses can be written as

$$R_{12}(\tau) = \int_{-\infty}^{\infty} I_1(t) I_2(t + \tau) dt \quad (3)$$

It can be shown that the resultant measured signal from the autocorrelator gives

$$S(\tau) = R_{CC}(\tau) + R_{TT}(\tau) + R_{CT}(t - \tau_d) + R_{TC}(t + \tau_d), \quad (4)$$

where R_{CC} , R_{TT} are autocorrelation functions of the clock and transmitter respectively, and R_{CT} , R_{TC} are cross-correlation functions between the clock and the transmitter. When the relative timing jitter is greater than the maximum autocorrelation width, the cross-correlation components of the signal will be proportional to the cross-correlation convolved with the jitter distribution. Thus, measuring the FWHM of the cross-correlation peak will allow us to measure the relative timing jitter. Assuming a Gaussian distribution for the timing jitter $J(t)$, the jitter can be calculated from

$$\tau_{CT}^2 = \tau_{CC}^2 + \tau_{TT}^2 + \tau_J^2. \quad (5)$$

4.2 Timing Jitter vs. Injected Power

We expect that the pulse to pulse timing jitter varies with the optical power of the injected data stream. We attenuated the injected optical power with a variable neutral density filter as we observed the RF spectrum and the temporal pulse pattern. When the injected power was small, the clock signal appeared to be unsynchronized with the data signal, and the RF spectrum had the large phase noise sidebands characteristic of a passively modelocked laser. When we increased the injected power, the clock pulses appeared synchronized with the data, and the RF spectrum had the low phase noise characteristic of the hybrid modelocked data pulses. Our experiment reveals that the clocking system shows a threshold behavior, with the clock oscillator being completely locked to the data stream or completely unlocked, i.e. free running, depending on the injected power. The timing jitter remains small with sufficient injected power and jumps to a significantly larger value when the injected power decreases below the locking threshold. Near the threshold, it is difficult to measure the timing jitter because the system shows erratic behavior. Figure 9 shows a single sweep RF spectrum of the clocking signal at threshold. The actual RF spectrum observed on the spectrum analyzer fluctuates erratically when the system is operating near the threshold.

The clocking threshold varies greatly with a multiple of parameters, including alignment of the clocking system, coupling with the transmitter, quality of the focus point on the saturable absorber, and pulse quality of the injected data stream. The smallest stable threshold we observed was 58 μW of injected optical power. However, much smaller thresholds were observed for very brief times, suggesting that it is possible to decrease this power significantly. Lack of mechanical mounts capable of providing the necessary degree of mechanical stability may be responsible for the higher threshold. It is desirable to reduce this threshold as much as possible to reduce the amount of power that is removed from the data stream to lock the clocking system.

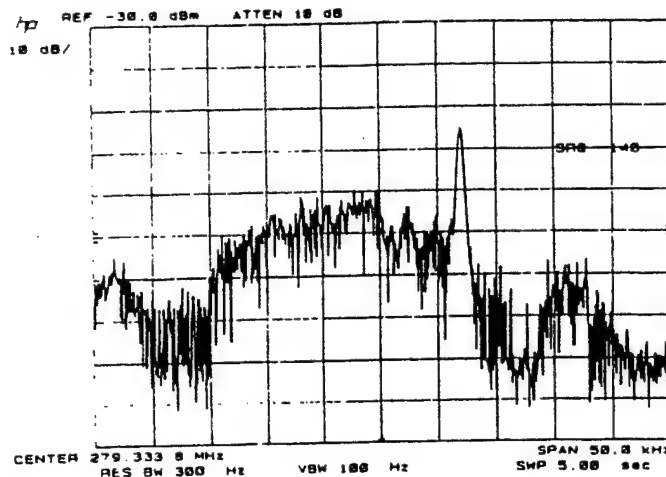


Figure 9: RF spectrum of the clock oscillator near clocking threshold shows erratic behavior.

4.3 Timing Jitter vs. Frequency Detuning

There may be small variations between the repetition rates of the transmitter system and the clocking system. In a multi-node optical communications network there may even be several sources of data all operating at slightly different repetition rates. It is important that the clocking system be robustly able to lock to each of these repetition frequencies independently. In our experimental demonstration, we were able to drive the transmitter system to operate at different frequencies by adjusting the frequency of the signal generator that provides the RF bias modulation for active modelocking.

Given that the system has a fixed timing jitter, Figure 10a shows the amount of frequency detuning possible with a given injection power. As this suggests, a wide detuning range can be obtained simply by maintaining a large enough injected power. With an injected power of about 700 uW, over 200 kHz of detuning, or a fractional bandwidth of 7.1×10^{-4} , is possible. Figure 10b shows two RF spectra at the maximum and minimum frequencies of the detuning range. Frequency detuning shows the same threshold behavior as varying the injected power. The phase noise sidebands stay small until the transmitter is tuned outside of the maximum range, then the phase noise becomes large as the clock reverts to “free-running” in passively modelocked operation.

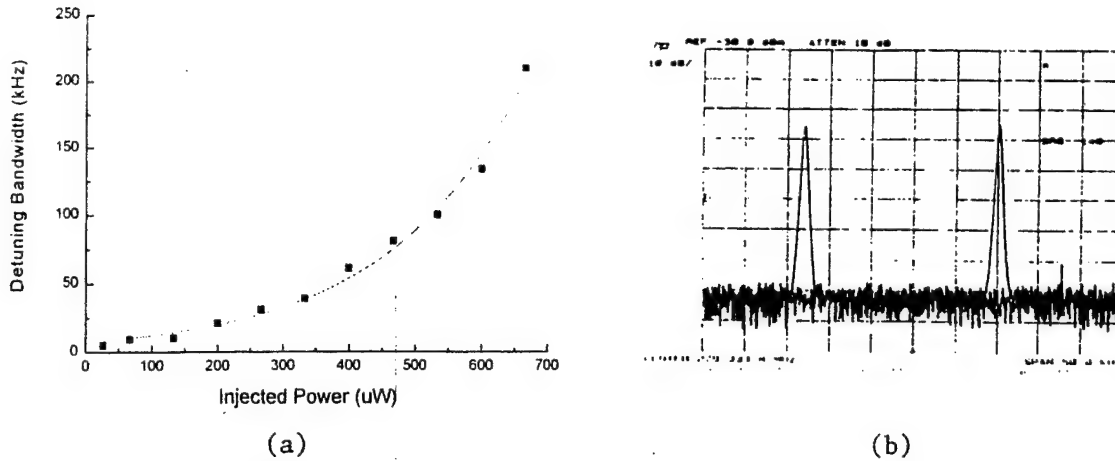


Figure 10: (a) Frequency Detuning vs. Injected Power with exponential fit (b) RF spectrum at the maximum and minimum of the detuning range.

4.4 Timing Jitter vs. Wavelength Detuning

There may also be slight variations in the wavelength of the injected data stream and the operating wavelength of the clock regeneration system. In the case of WDM, it would be desirable to use the same clock recovery system for multiple wavelength channels. The clocking system will work robustly for a range of wavelengths as long as the wavelengths are within the gain bandwidth of the TWA and/or within the excitonic absorption band of the saturable absorber depending on the clocking scheme. If the clocking data is injected directly onto the saturable absorber, then it is only necessary to be within the absorption band of the absorber. If it is also injected through the diode for gain modulation, then the bandwidth of the laser diode must be taken into account.

To perform the wavelength detuning experiment, it will be necessary to accurately control the wavelength of the transmitter laser by using an intracavity filter. A narrowband filter will be placed inside the cavity to force the system to operate at the desired wavelengths. The filter can be angle tuned to change the operating wavelength. The system can be tuned through the spontaneous emission bandwidth of the laser diode, which is 20 nm. Figure 11 shows a schematic diagram of the wavelength tunable laser system.

We will measure the timing jitter as we vary the wavelength and determine the wavelength detuning range, similar to the frequency detuning measurements shown in the previous section.

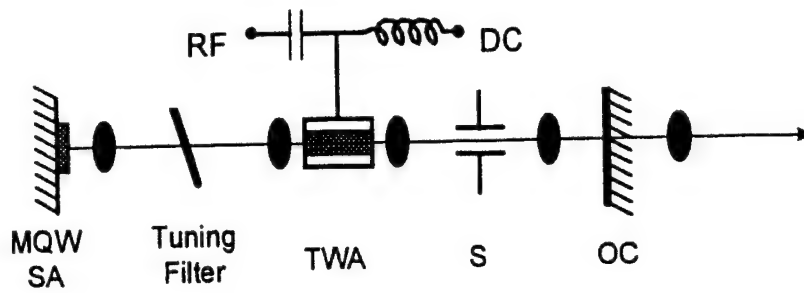


Figure 11: Wavelength tunable transmitter laser system

4.5 Timing Jitter vs. Bit Pattern

In all of the experiments we have performed, we have used an unmodulated data stream. The data bit pattern was a series of all "1"s. It is necessary to look at the timing jitter when the data stream is modulated with different bit patterns. It is likely that there will be extra timing jitter, and possibly some amplitude fluctuations on the extracted clocking signal.

To act as an amplifier/modulator the TWA is modulated with short (4 ns) electrical pulses while the amplifier is DC biased below the amplification threshold. All pulses are suppressed except for the ones that pass through the amplifier at the same time as the electrical pulses. Figure 12 shows the output of the pulse slicer. It is operating at one tenth of the fundamental repetition rate.

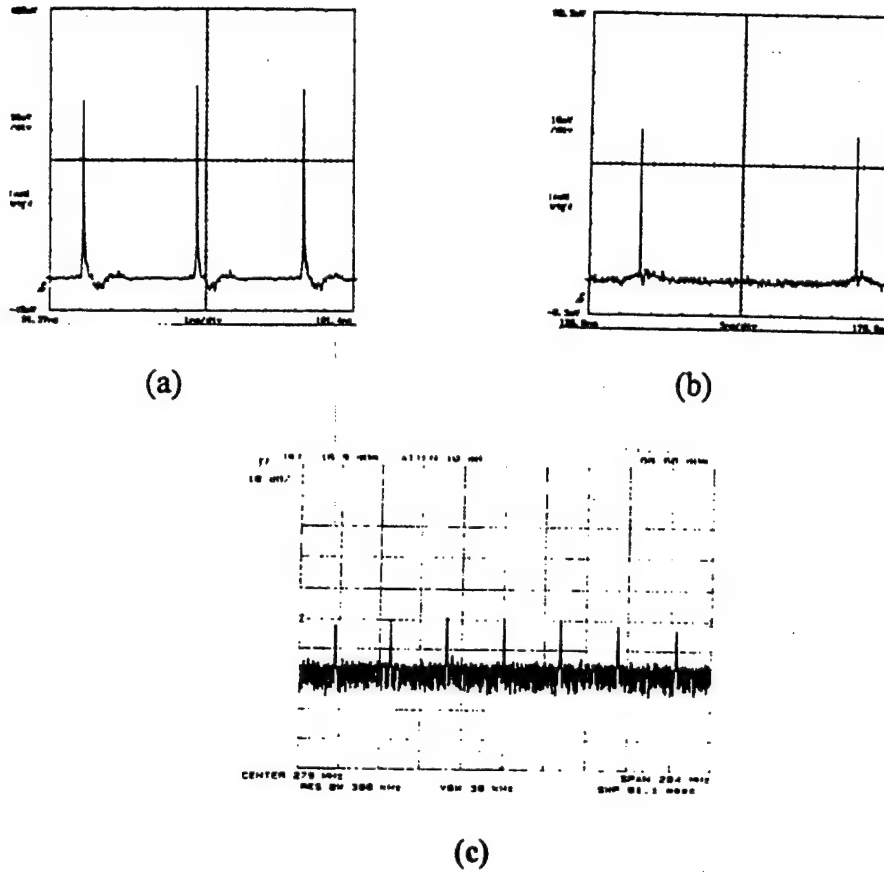


Figure 12: Pulse Slicer (a) pulses before being modulated (b) 1 out of 10 pulse slicing (c) RF Spectrum after slicing showing modulation.

It will also be significant to measure the lock-up time, or the amount of time it takes for the clock to generate a synchronized clocking signal after the data pulses starts to be injected. This will have significant impact on the latency of the system.

This can be done by sending a short string of pulses ("1"s) separated by a long delay ("0"s). If the system locks onto the pulses, there will be a decrease in timing jitter. If they do not, the timing jitter will stay characteristic of the passively modelocked oscillator. The number of pulses in the data stream can be increased until synchronization is observed. It is expected, due to the strong nonlinearities in the laser diode and the saturable absorber, that synchronization should occur within a few pulses, perhaps even after just one pulse.

The system ring-down time, or the time it takes for the system to lose synchronization after the data stops, is also important to characterize. After the data stops, random fluctuations in the passively modelocked clock laser will cause it to drift out of synchronization. A long ring-down time allows the system stay accurately synchronized when the data stream contains long

strings of "0"s. It may also decrease latency if the clock pulses stay synchronized even when there is no data present.

The ring-down time can be measured by sending a long stream of pulses ("1"s) followed by a short delay ("0"s). If the clock loses synchronization quickly, we will observe extra timing jitter. The timing jitter will be measured with increasing delay lengths to measure the system's performance over time after the data stream stops.

5.0 Future Work

As suggested in the previous sections, there is still much to be done with the system as it is currently configured. A better understanding of the dynamics of clock recovery is necessary in order to find ways to improve the system's performance. We may also want to look at different ways we can inject the data stream, including changing its polarization to make it orthogonal to the clock pulses. This may decrease interaction between the injected pulses and the clock pulses inside the laser diode.

We would like to demonstrate the system at higher repetition rates. It is perceived that a commercially viable version of this type of clock recovery system would be monolithically integrated, or compacted with miniature bulk optics. In either case, to increase the repetition rate, the cavity length must be decreased, or the clock must be operated with multiple pulses in the cavity at the same time.

In addition, we plan to perform similar oscillator synchronization experiments with TWA's at a wavelength of $1.5\text{ }\mu\text{m}$. This wavelength is of greater significance, and of greater application in optical photonic systems.

6.0 References

- ¹ D.H. Hartman, "Digital high speed interconnects: a study of the optical alternative," *Optical Eng.*, vol. 25, no. 10, pp. 1086-1102, 1986.
- ² P. Delfyett, "Hybrid modelocked diode lasers for synchronous optical network applications," *SPIE Proc.* Vol. 2116, 1994.
- ³ T. Ono, Y. Yamabayashi, and Y. Sato, "5 Gbits/s all-optical clock recovery using a dual modelocking technique," in *OFC94*, paper ThM3, 1994.
- ⁴ M. Jinno, and T. Matsumoto, "Optical retiming regenerator using 1.5 μm wavelength multielectrode DFB LD's," *Electron Lett.*, vol. 25, no. 20, pp. 1332-1333, 1989.
- ⁵ P.E. Barnsley, H. J. Wickes, G.E. Wickens, D.M. Spirit, "All-optical clock recovery from 5 Gbit/s RZ data using self-pulsating 1.56 μm laser diode," *IEEE Photon. Technol. Lett.*, vol 3, p942-945, 1991.
- ⁶ U. Feiste, D.J. As, A. Ehrhardt, "18 GHz all-optical frequency locking and clock recovery using a self-pulsating two-section DFB-laser," *IEEE Photon. Technol. Lett.*, vol. 6, p106-108, 1994.
- ⁷ A. Ellis, K. Smith, and D. Patrick, "All optical clock recovery at bit rates up to 40 Gbit/s," *Electron. Lett.*, vol. 30, pp. 151-152, 1994.
- ⁸ D. Patrick, and R. Manning, "20 Gbit/s all-optical clock recovery using semiconductor nonlinearity," *Electron. Lett.*, vol.30, pp. 151-152, 1994.
- ⁹ V.B. Khalfin, J.M. Arnold, and J.H. Marsh, "A theoretical model of synchronization of a modelocked semiconductor laser with an external pulse stream," *IEEE Sel. Topics Quant. Elect.*, vol. 1, no. 2, 1995.
- ¹⁰ B.K. Mathason, P.J. Delfyett, "Applications of ultrafast modelocked laser diodes in synchronous optical networks," *SPIE Proc.* Vol. 2749, p 134-140, 1996.
- ¹¹ D.S. Chemla, D.A.B. Miller, P. Smith, "Room temperature excitonic nonlinear absorption and refraction in GaAs/AlGaAs multiple quantum well structures," *IEEE J. Quantum Electron.*, vol QE-20, pp 265-275, 1984.
- ¹² P.J. Delfyett, D.H. Hartman, and S.Z. Ahmad, "Optical Clock Distribution Using a Modelocked Semiconductor Laser Diode System," *J. Lightwave Tech.*, vol. 9, no. 12, pp.1645-1649, 1991.
- ¹³ See, for example, P. Bhattacharya, Semiconductor Optoelectronic Devices, Prentice Hall, Englewood Cliffs, NJ, 1994.
- ¹⁴ D. von der Linde, "Characterization of the Noise in Continuously Operating Modelocked Lasers," *Appl. Phys. B*, vol 39, pp 201-217, 1986.

- ¹⁵ U. Keller, K.D. Li, M. Rodwell, D. Bloom, "Noise Characterization of Femtosecond Fiber Raman Soliton Lasers," *IEEE J. Quantum Electron.*, vol. 25, pp. 280-287, 1989.
- ¹⁶ P.J. Delfyett, L.T. Florez, N. Stoffel, et al. "High-Power Ultrafast Laser Diodes," *IEEE J. Quantum Electron.*, vol 28, pp 2204-2219, 1992.
- ¹⁷ P.J. Delfyett, "High Power Ultrafast Semiconductor Injection Diode Lasers," in Compact Sources of Ultrashort Pulses, Cambridge University Press, New York, NY, pp 274-325, 1995.

MISSION OF ROME LABORATORY

Mission. The mission of Rome Laboratory is to advance the science and technologies of command, control, communications and intelligence and to transition them into systems to meet customer needs. To achieve this, Rome Lab:

- a. Conducts vigorous research, development and test programs in all applicable technologies;
- b. Transitions technology to current and future systems to improve operational capability, readiness, and supportability;
- c. Provides a full range of technical support to Air Force Material Command product centers and other Air Force organizations;
- d. Promotes transfer of technology to the private sector;
- e. Maintains leading edge technological expertise in the areas of surveillance, communications, command and control, intelligence, reliability science, electro-magnetic technology, photonics, signal processing, and computational science.

The thrust areas of technical competence include: Surveillance, Communications, Command and Control, Intelligence, Signal Processing, Computer Science and Technology, Electromagnetic Technology, Photonics and Reliability Sciences.